

Delta weights for footprint suppression in 3D prestack migration

Joanna K. Cooper, Gary F. Margrave, and Don C. Lawton

ABSTRACT

When compared to prestack-migrated images of a fully-sampled (“exhaustive”) numerical model seismic dataset, images from decimated (under-sampled) datasets display acquisition footprint artefacts. In this study, a weighting scheme for prestack Kirchhoff migration that attempts to compensate for irregular illumination of image points, which was previously shown to have promise in 2D, was implemented in 3D using MATLAB. The method was applied to the exhaustive and decimated datasets, with the purpose of examining its ability to suppress footprint artefacts. The scheme involves hit counting of delta angles for traces input to the migration, where delta describes the dip and azimuth of the vector bisecting the source-to-image-point and receiver-to-image-point rays. Though the method does not address footprint related to the aperture of the survey, it does appear to reduce the severity of footprint artefacts consisting of periodic amplitude variations in the interior of the survey, without losing the ability to resolve edges in the migrated images. The method produced results that are better than a comparable common-offset-weighted migration.

INTRODUCTION

Previously (Cooper et al., 2007, 2008), we described a numerical modelling study initiated with the goal of studying acquisition footprint. The premise behind the study is to model 2D and 3D exhaustive datasets, meaning datasets with source and receiver intervals small enough to sample the seismic wavefield without aliasing in any spatial dimensions. Then, the exhaustive datasets are decimated to produce survey designs more typical of those used in the field. Finally, the exhaustive and decimated datasets are processed, including stacking, poststack migration, and prestack migration to examine the resulting footprint artefacts. The 2007 simulations demonstrated that footprint in 2D can manifest in prestack-migrated images as residual migration wavefronts, as insufficient spatial sampling does not allow for proper constructive and destructive interference. In 3D, the simulations demonstrated that the choice of prestack migration algorithm is an important factor in determining the severity and character of footprint in the prestack-migrated images. In 2008, we described the implementation of a particular prestack migration weighting scheme in 2D based on equalizing angular contributions at each image point; the angle in question is delta, the dip of the vector bisecting the source-to-image-point and receiver-to-image-point rays. The method appears to reduce the severity of 2D footprint artefacts. In this paper, we report on the extension of the method to 3D and present the results of 3D prestack migrations using this weighting scheme.

As described in Margrave and Cooper (2007), the model for the 2D simulations was 400m long with a single reflector at 200m depth in a $v(z)$ medium. The reflector consisted of a constant positive reflection coefficient, except for an opposite-polarity feature in the middle of the reflector, simulating a channel. The exhaustive dataset involved a shot spacing of 5m and a receiver spacing of 5m. Data were modelled using a Kirchhoff modelling algorithm in MATLAB. Figure 1 shows the results of prestack

migrations of the exhaustive dataset, as well as five decimated datasets, with shot spacings of 10m, 25m, 50m, 100m, and 200m. The prestack migration algorithm was a Kirchhoff shot-record migration with weights prescribed by Bleistein et al. (2001). Footprint artefacts are clearly visible in the more severely decimated datasets. Figure 2 shows the results of prestack migration using the delta-ratio prestack migration weights described by Cooper et al. (2008). The footprint artefacts are not as prominent. These results prompted us to attempt to extend the method to 3D to see if similar improvements could be achieved for 3D surveys. The delta-ratio weighting scheme is recapped below as we describe its extension to the case of 3D prestack migration.

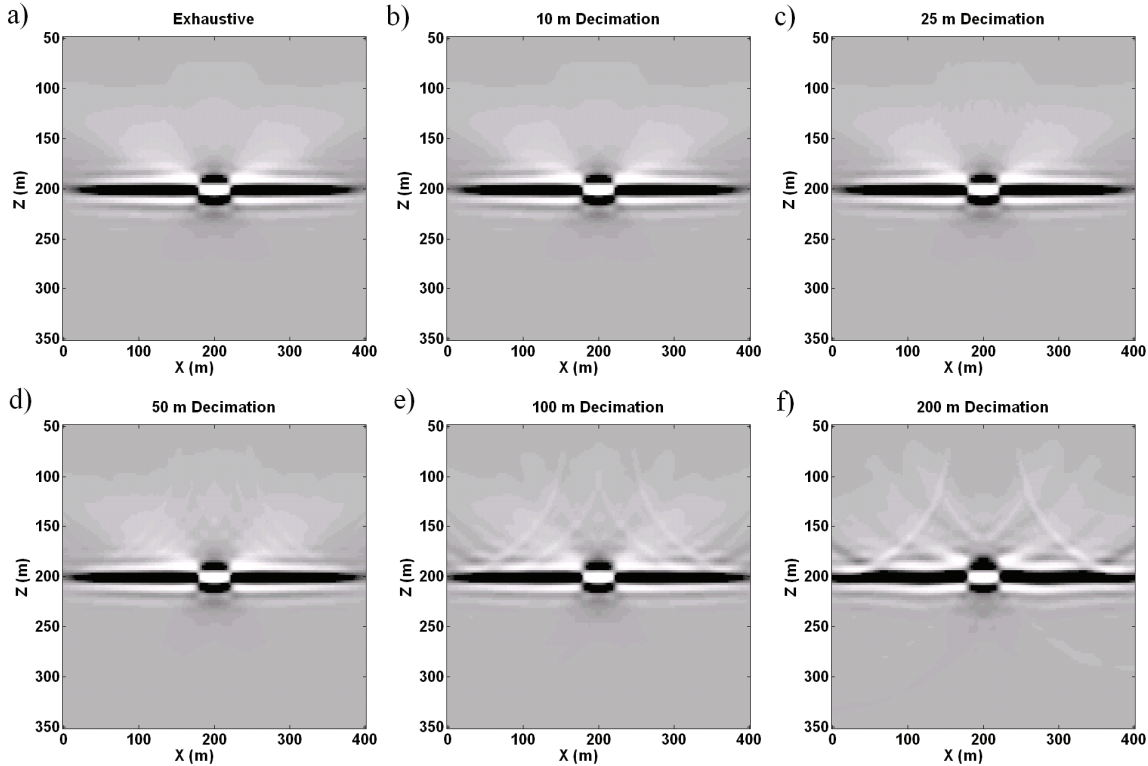


FIG. 1. 2D prestack migrations from Cooper et al. (2008). The exhaustive dataset (a) had a shot spacing equal to the receiver spacing. The five decimated datasets had shot spacings of twice (b), five times (c), ten times (d), twenty times (e), and forty times (f) the receiver spacing. Footprint artefacts consisting of residual migration wavefronts are observable in d) through f) and are also subtly present in c)

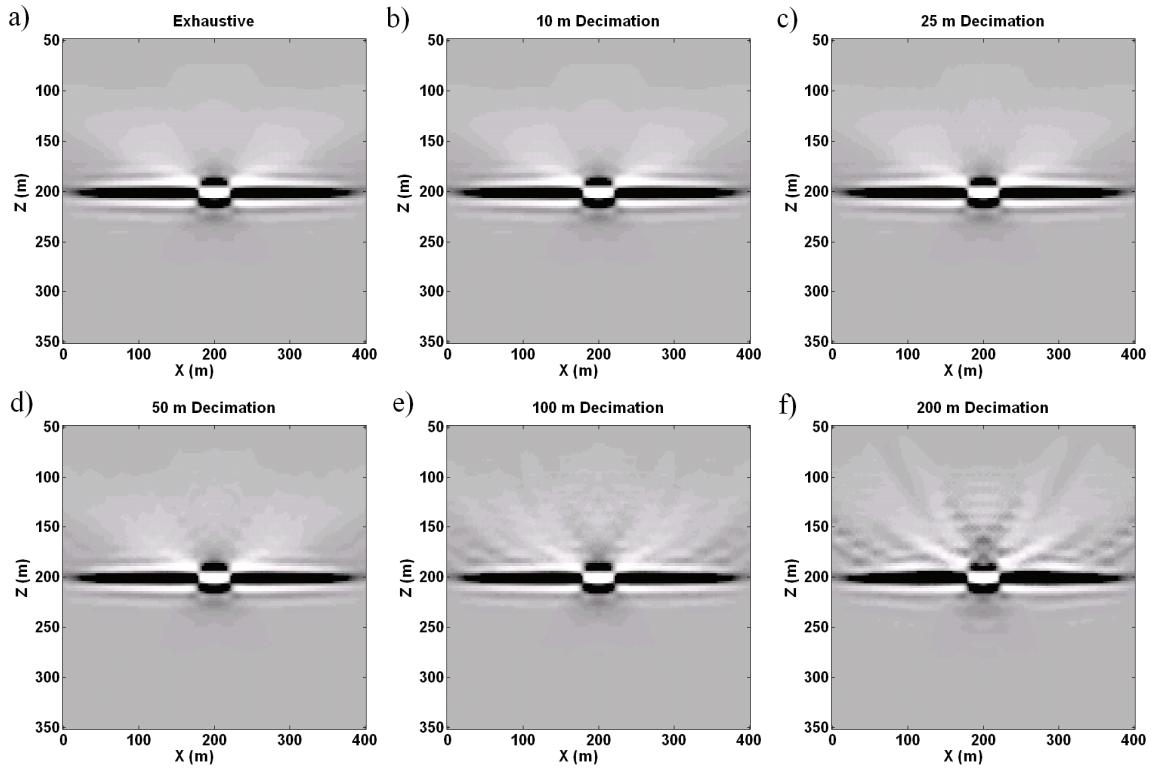


FIG 2. 2D prestack migrations of the exhaustive dataset (a) and the five decimated datasets (b-f) using delta-ratio weights, from Cooper et al. (2008). Compared to Figure 1, residual migration wavefronts are less pronounced.

The model for the 3D simulations, as described by Margrave and Cooper (2007), was 400m by 400m in area, with three reflectors in a $v(z)$ medium, at 100m, 180m, and 200m. The two shallow reflectors were featureless, meaning that they had constant reflection coefficients. The 200m deep reflector had a sinuous channel feature and several point diffractors, as shown in Figure 3. The exhaustive and decimated geometries are displayed in Figure 4. The exhaustive survey had source and receiver spacings of 10m in both x and y directions. The decimated survey, familiar from the previous studies, had an orthogonal design, with source and receiver line spacings of 80m, but with source and receiver spacings of 10m along those lines. Figure 5 shows the results of Kirchhoff prestack migration with Bleistein weights, as described by Cooper et al. (2007). The goal of the current study was to implement the delta weighting scheme in 3D and compare the footprint artefacts in the resulting migrations to those in Figure 5.

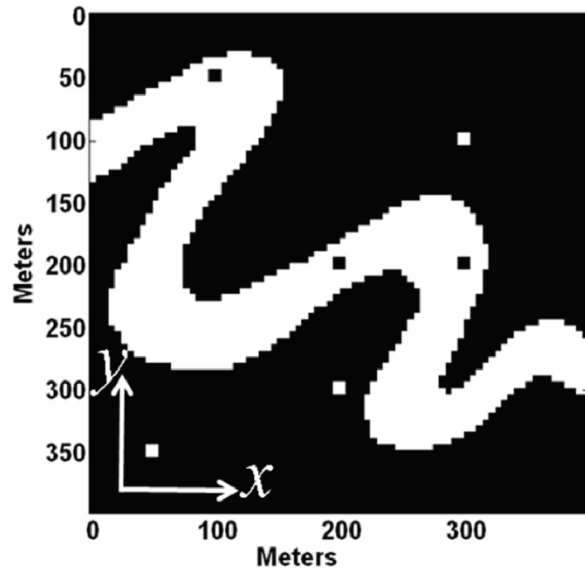


FIG. 3. Reflectivity map of 200m deep reflector in 3D model.

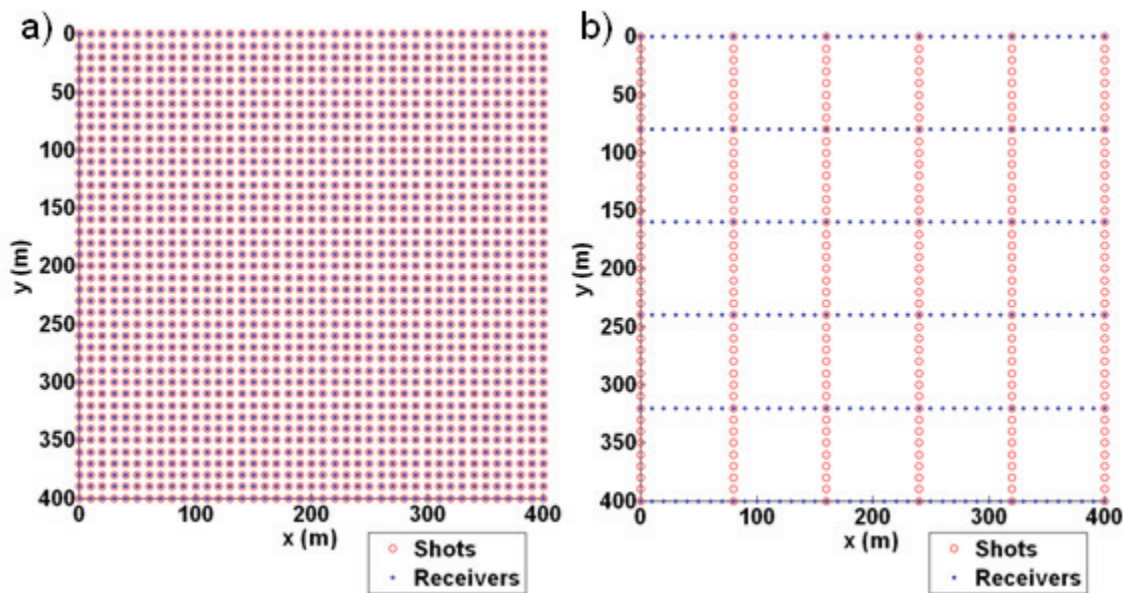


FIG. 4. Survey geometries of exhaustive (a) and decimated (b) datasets.

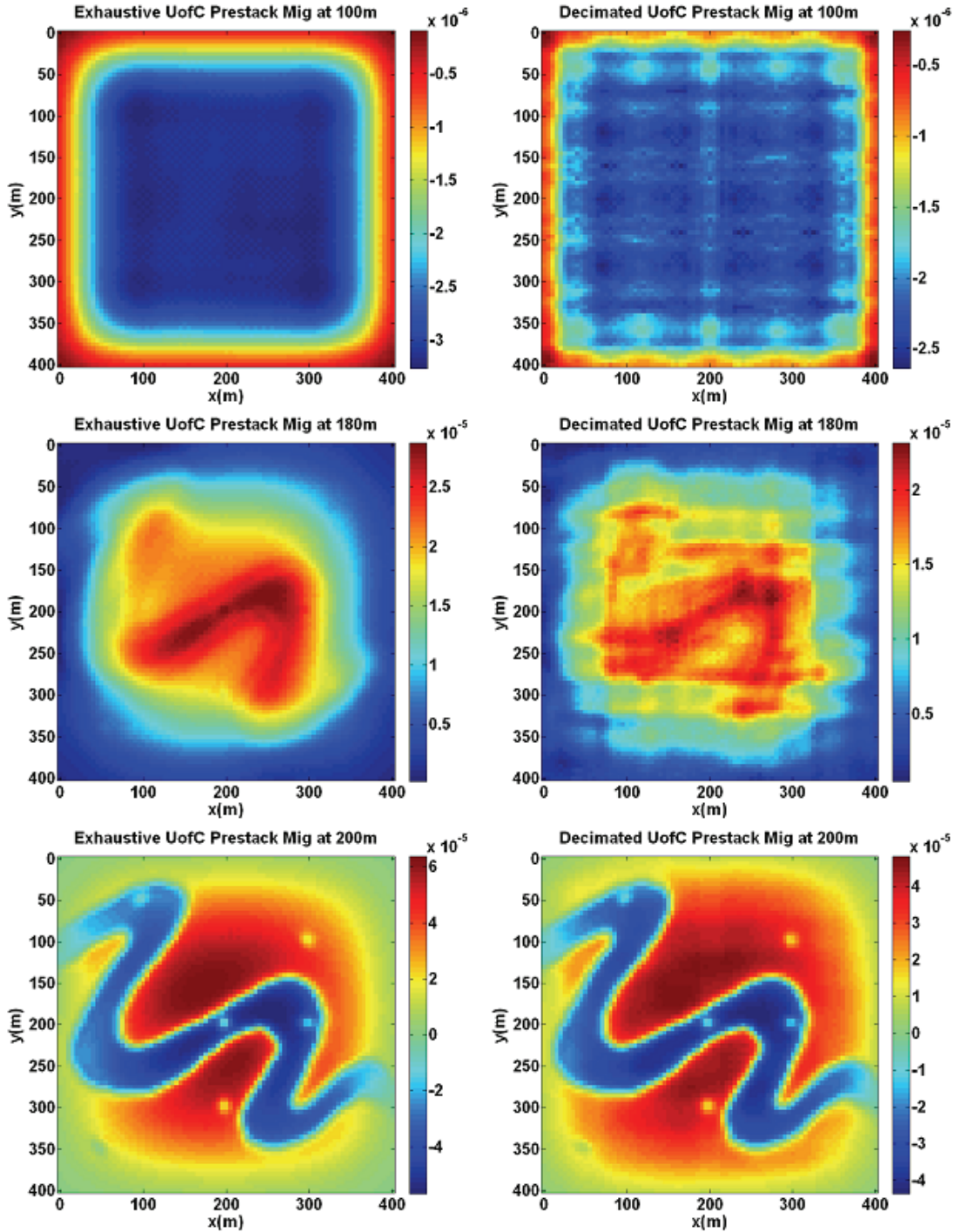


FIG. 5. Depth slices from 3D prestack migrations at the 100m featureless reflector (top row), the 180m featureless reflector (middle row), and the channel reflector (bottom row) from Cooper et al. (2008). Images in the left-hand column are from the exhaustive survey; those from the right-hand column are from the decimated survey.

METHOD

As described by Cooper et al. (2008), the prestack migration weighting scheme is based on the concept of compensating for irregular illumination of each image point.

Incomplete sampling of the wavefield in surface coordinates (shot and receiver x and y) correspondingly produce irregular sampling on the hemisphere surrounding the image point. We describe the sampling of the image hemisphere using the concept of delta angles. Delta describes the orientation of the vector that bisects the source-to-image-point and receiver-to-image-point rays (Figure 6). In 3D, delta has both a dip and an azimuth component. For a given image point, each prestack trace (each source-receiver pair) defines a single delta. As shown in Cooper et al. (2008), decimated survey geometries produce delta angle distributions that are different than the exhaustive survey. We hypothesize that footprint artefacts are a result of this delta angle imbalance, and that by weighting traces such that the ideal delta angle sampling is re-established, the footprint artefacts will be reduced.

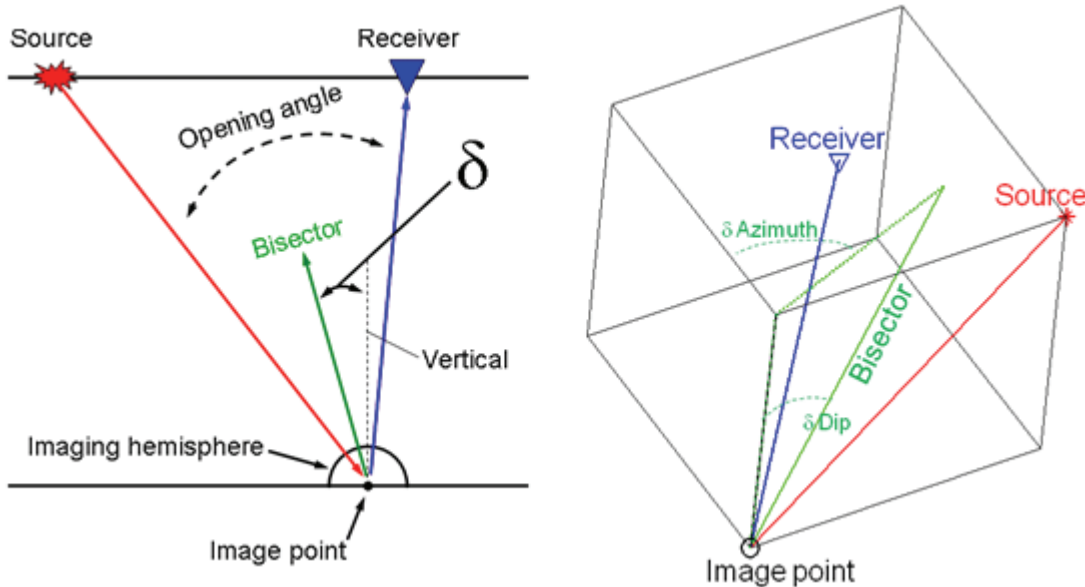


FIG. 6. Delta angles in 2D and 3D, defining the orientation of the vector bisecting the opening angle between source and receiver rays.

An important consideration in the extension of the delta angle concept from 2D to 3D is the azimuth. In 2D, the source, receiver, and image point are all in a single vertical plane, so the concept of azimuth is not required, other than keeping track of the sign of the delta dip angle. Cooper et al. (2008) found that in 2D, ignoring the sign of delta produced poorer results than those produced when the sign of delta was included. This suggests that in 3D, azimuthal variations in delta distributions will also be significant.

Prestack Kirchhoff migration is simply a weighted sum at each image point. Weights include those that compensate for spreading and obliquity. As described by Cooper et al. (2007, 2008), we use the shot-record migration weights prescribed by Bleistein et al. (2001). However, to compensate for the delta angle sampling irregularities, we introduce an additional weight to be applied to each trace as it is summed at the image point. The weights are pre-calculated by determining the hit counts in defined delta angle bins on imaging hemisphere. We are able to pre-calculate weights since they are just based on the collection of source and receiver coordinates in the survey. As described by Cooper

et al. (2008), we consider two types of weights: delta-fold weights and delta-ratio weights. The delta-fold weight for a given trace can be written as

$$W_k(\underline{x}) = 1/n(\underline{x}, \delta_k), \quad (1)$$

where $n(\underline{x}, \delta_k)$ is the hit count in bin δ_k for the image point at position (\underline{x}) . In this way, delta-fold weights cause all delta bins to contribute equally to the sum at the image point. The delta-fold weights are only a function of the decimated survey geometry. In contrast, delta-ratio weights involve hit counts from both the decimated and exhaustive surveys. The delta-ratio weight for a trace is

$$W_k(\underline{x}) = n_{exh}(\underline{x}, \delta_k)/n(\underline{x}, \delta_k), \quad (2)$$

where $n(\underline{x}, \delta_k)$ is the hit count in bin δ_k for the image point at (\underline{x}) in the decimated survey, and $n_{exh}(\underline{x}, \delta_k)$ is the same, but for the exhaustive survey. The delta-ratio weights, instead of making the contributions from all delta bins equal, makes the contributions from each delta bin equal to what it would have been in the exhaustive survey. Once calculated, the delta-fold or ratio weights are implemented in the prestack shot-record migration sum according to

$$Im(\underline{x}) = \sum_{j \text{ shots}} [\sum_{k \text{ bins}} (W_k(\underline{x}) * \varphi_j(\underline{x}, \delta_k))], \quad (3)$$

where $Im(\underline{x})$ is the migrated image at the image point at (\underline{x}) and $\varphi_j(\underline{x}, \delta_k)$ is the j -th migrated shot record, limited to those traces whose delta angles fall in bin δ_k . In practice, we produce $\varphi_j(\underline{x}, \delta_k)$ by migrating each shot record into delta-limited output volumes.

RESULTS

Figure 7 shows the results from prestack migrations of the decimated dataset using delta-ratio weights with different choices of delta binning. In all cases, the delta dip binning was in 5 degree bins, which was the optimal bin width in the 2D simulations from Cooper et al. (2008). However, the azimuthal binning was different: in (a) there was no azimuthal binning; in (b) there were 4 azimuth bins; in (c), 8 azimuth bins; and in (d), 16 azimuth bins. Compared to Figure 5, the delta-ratio weighted migrations show fewer footprint artefacts than the migrations without delta weights. This is especially apparent on the 100m and 180m deep featureless reflectors. At the channel level, the delta-ratio weight images show that the weighting scheme preserves the resolution of the channel edges and point diffractors. Comparing the different azimuth binnings, there is a significant improvement in the images moving from 1 azimuth bin to 4 azimuth bins. There is also an improvement when moving to 8 azimuth bins. However, using 16 azimuth bins does not produce much of an improvement over 8 azimuth bins. These results are similar to the 2D simulations (Cooper et al., 2008), where considering the sign of delta (equivalent to keeping track of azimuth) was more effective than considering only the absolute value of delta. The 3D results are also consistent with the findings in 2D that there was an optimal bin size; finer binning generally produced better results. However, at a certain point, the bins were too small to be effective. In 3D, the 16 azimuth bins are small enough to not yield any considerable improvement over 8 azimuth

bins, but are not fine enough to produce degradation of the image, as was seen with the very fine delta dip binning in 2D.

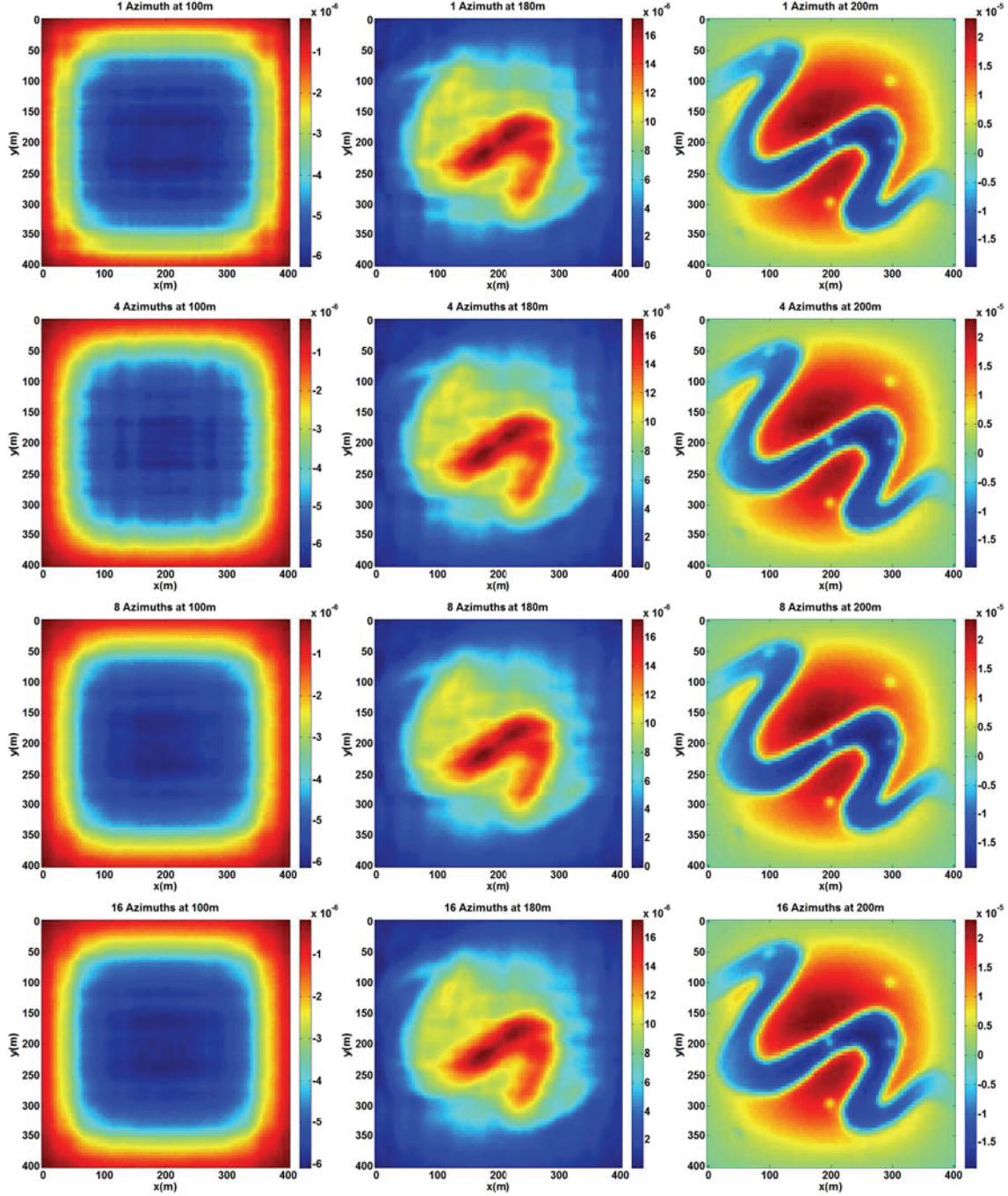


FIG. 7. Depth slices from delta-ratio weighted prestack migrated images at the three reflectors: 100m featureless (left), 180m featureless (middle), and 200m channel (right). From top to bottom, the azimuthal binning involved 1, 4, 8, and 16 azimuth bins.

Figure 8 shows depth slices from the prestack migration using the delta-fold weights for the decimated dataset and the same binning that was used to create the 8 azimuth bins delta-ratio weight image from Figure 7. As observed using the delta-fold weights in 2D

by Cooper et al. (2008), the weights are very successful in removing the aperture imprint of the survey; however, they produce edge artefacts which appear as lineations on the two shallow slices in Figure 8. The 100m deep featureless reflector also displays some residual internal amplitude variations or footprint. Perhaps of even more significance is something not observed previously in 2D but very apparent in 3D, namely that the delta-fold weights also appear to reduce resolution of the channel edges and especially of the point diffractors, compared to the migrations with no delta weights and those with the delta-ratio weights. As a result, this weighting scheme does not seem to be successful.

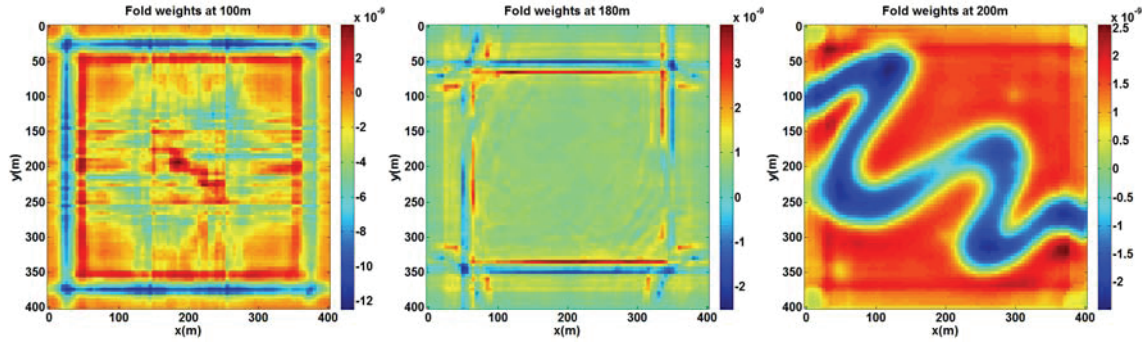


FIG. 8. Depth slices at 100m, 180m, and 200m from delta-fold weighted prestack migrations of the decimated dataset.

Though the delta-ratio weighting scheme does appear to reduce footprint artefacts, the Cooper et al. (2007) simulations demonstrated that industrial common-offset and common-offset-vector migration algorithms were also successful in reducing the artefacts. So, we compared the delta-ratio weighting technique to one of these more conventionally used methods. However, because the delta-ratio weight shot-record migration algorithm we are using does not include any optimizations generally incorporated in industrial algorithms (such as smoothing of weights, borrowing of traces from adjacent bins to fill holes, etc.), we wanted to make an objective comparison. So, we coded a version of a Kirchhoff common-offset-weighted prestack migration in MATLAB, such that it was of comparable sophistication to our shot-record migration. As described by Cooper et al. (2007), the method involves computing offset-limited fold volumes, and then pre-weights traces by the offset-limited fold that corresponds to the offset bin into which the trace falls. Because the weights are applied before migration, the migration does not technically need to be performed in the common-offset domain; in fact, in our implementation the algorithm is still a shot-record migration. An important parameter in the method is the choice of offset bins. The idea is to have as many offset bins as possible, while still keeping each bin populated at every midpoint, or as close as possible. Here we just show three choices of binning: a single offset bin (which amounts to just pre-weighting the traces by conventional CMP fold), two offset bins of 0-250m and >250m, and six offset bins of 0-100m, 100-200m, 200-300m, 300-400m, 400-500m, and 500-600m. Figure 9 shows the results of these common-offset-weighted migrations. Even though these are likely not optimal choices of binning, the results using six offset bins show the ability of the method to compensate for aperture, still resolve edges very well, and do some internal footprint compensation.

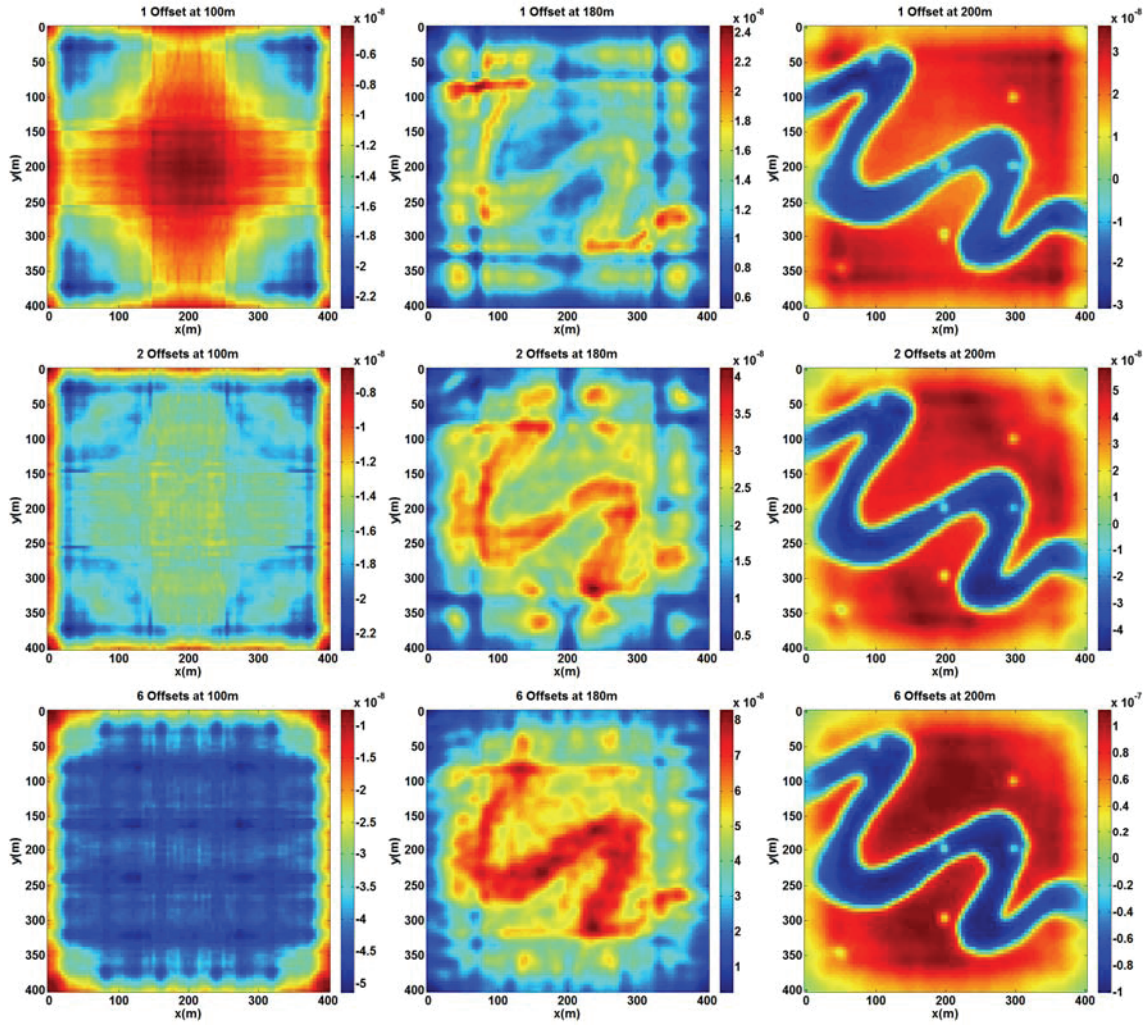


FIG. 9. Depth slices from common-offset-weighted prestack migrated images at the three reflectors: 100m featureless (left), 180m featureless (middle), and 200m channel (right). From top to bottom, the offset binning involved 1, 2, and 6 offset bins.

While qualitative comparisons are informative, differences in scaling of individual images can be misleading; as a result, it is useful to find a means to quantify the differences between the methods. The best way to do this is to compare the migrated images to the known answer, i.e. the true reflectivity slices (e.g. Figure 3 for the channel level). One complication in the case of the delta-ratio weights is that the aperture imprint of the survey is still quite strong, meaning that those differences will dominate the comparison between migrated result and true reflectivity. In order to be able to compare the delta-ratio method to the other weighting schemes, we attempted to remove the aperture imprint on the ratio-weighted slices. The aperture imprint should be a smooth, symmetric amplitude decay away from the centre of the survey area. The approach we took was to create an estimate of the aperture imprint by severely smoothing the absolute value of the migrated slice via 2D convolution with a boxcar. Then, we divided the migrated slice by this aperture estimate, to produce an aperture-removed image. Figure 10 shows the aperture imprint estimate and the results of its removal for the 8 azimuth bin delta-ratio weight migrations at the three reflectors. By removing the aperture imprint,

the pure internal footprint artefacts are isolated and it allows for the direct comparison of the three weighting schemes. Figure 11 shows the difference between the true reflectivity and the migrated images using delta-ratio weights, delta-fold weights, and common-offset weights, for the 100m and 180m deep featureless reflectors as well as the 200m deep channel reflector. The differences are expressed in percent, after a bulk scaling of the mean of each migrated slice to match the mean amplitude of the reflectivity slice. Aperture removal was performed on the delta-ratio and common-offset slices. The delta-ratio and delta-fold images had 8 azimuth bins; the common-offset images had 6 offset bins. Examination of the channel reflector shows the ability of each method to resolve edges and points, whereas the featureless reflectors reveal the severity of the internal periodic amplitude variations. From these results, the delta-ratio weight method appears to produce the images with the least residual footprint compared to the migration without additional weights and the two other weighting schemes.

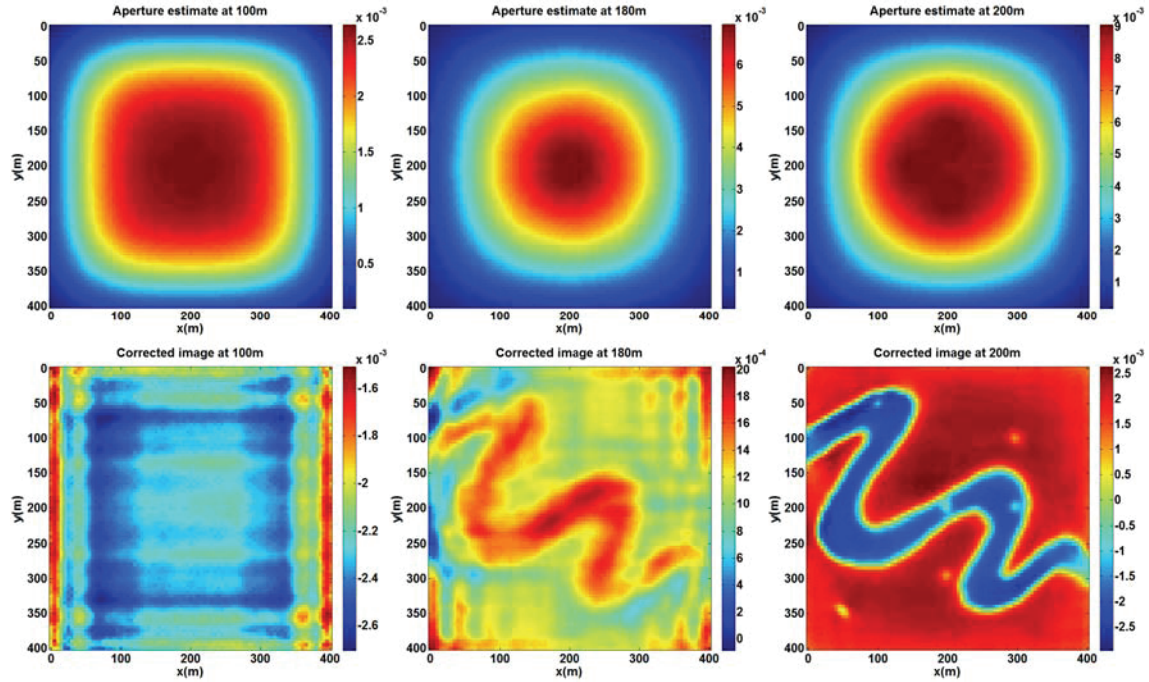


FIG. 10. Aperture estimate (top) and aperture-removed migrated depth slices (bottom) at 100m, 180m, and 200m for the delta-ratio weighted prestack migration of the decimated dataset with 8 azimuth bins.

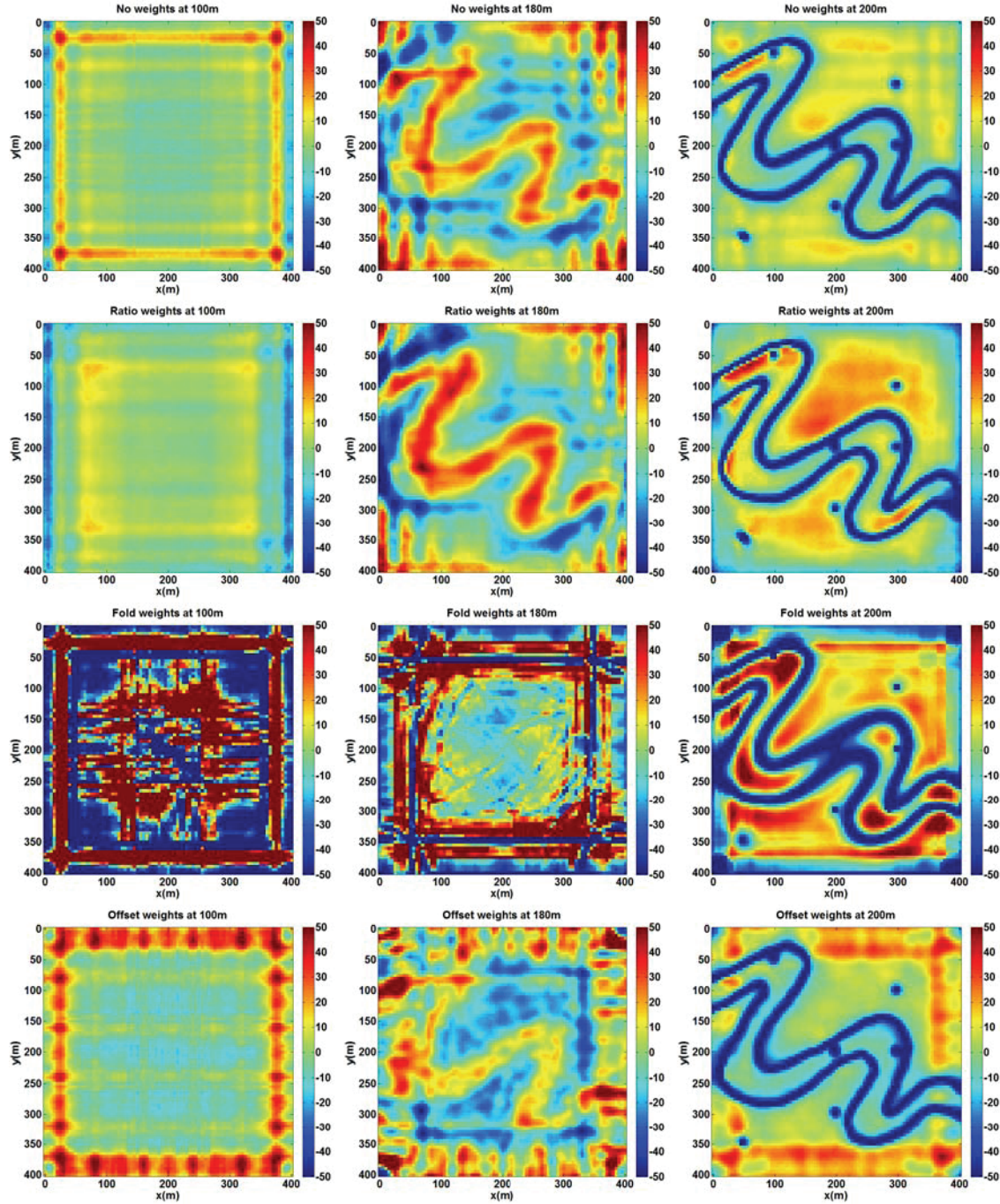


FIG. 11. Percent difference between migrated depth slices and the true reflectivity at 100m (left), 180m (middle), and 200m (right). Top to bottom: no weights (reference), delta-ratio weights, delta-fold weights, and common-offset weights.

Since the severity of the footprint in a migrated image is a function of not only the migration algorithm but also the survey geometry, we wanted to examine the performance of the delta-ratio weighting with a different sampling decimation. Figure 12 shows two alternate decimated surveys, which are identical to the original decimated survey from Figure 4 except that they contain a hole in the shot coverage, as might occur in the presence of some obstacle in the field. One version (Figure 12a) involves shot

lines that end abruptly at the obstacle, while the other (Figure 12b) has shot lines that smoothly bend around the obstacle. These surveys are of course not the only possibility for another survey geometry, but they do serve as a test of the weighting scheme in a situation with slightly more irregular sampling, rather than just sparse but still regular sampling.

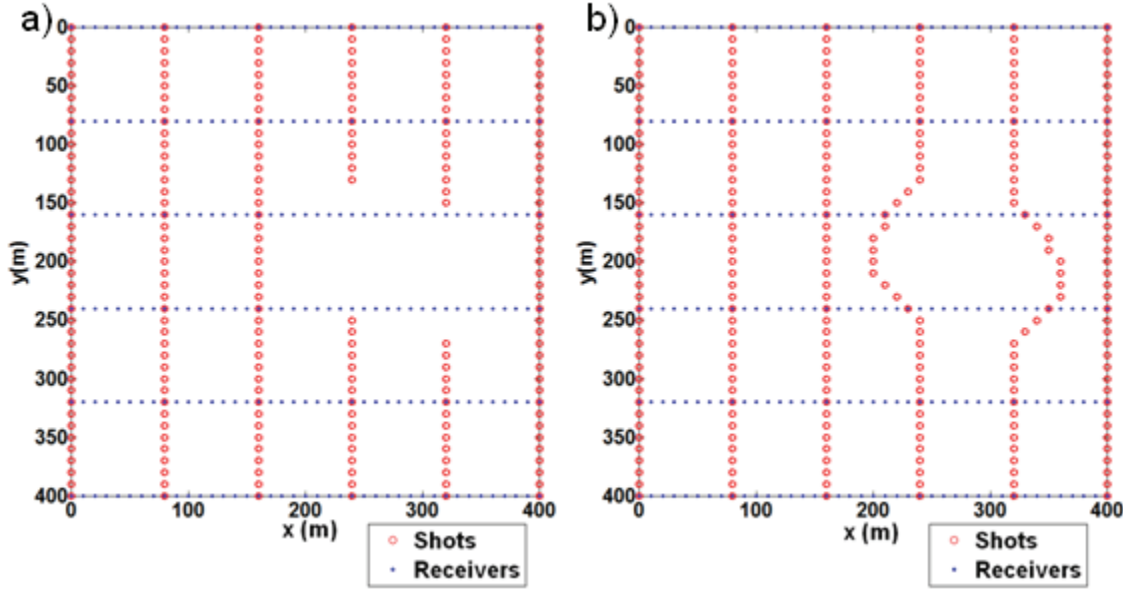


FIG. 12. Geometry of decimated surveys with a hole introduced by removal of shots (a) and by skidding of shots (b).

Figures 13 and 14 show the results from the prestack migration of these new decimated datasets, for the case without weights (comparable to Figure 5), and the case with the three different weighting schemes (comparable to Figures 7, 8, and 9). Figures 15 and 16 show the percent difference plots comparing the migrations to the true reflectivity (comparable to Figure 11). The migrated images now display the effect of a hole in the survey, in addition to the effect of a regular decimation. The hole affects the amplitudes most dramatically on the 100m featureless reflector. At the channel level, the hole seems most apparent in the common-offset images. For these decimations, the delta-ratio weights again appear to improve the images of the 100m and 180m deep featureless reflectors, and they preserve resolution of the channel edges and point diffractors. Comparing the survey with removed shots to the one with skidded shots shows that the second method produces much better images with all of the migration algorithms. The delta-ratio weights outperform the common-offset weights for both surveys.

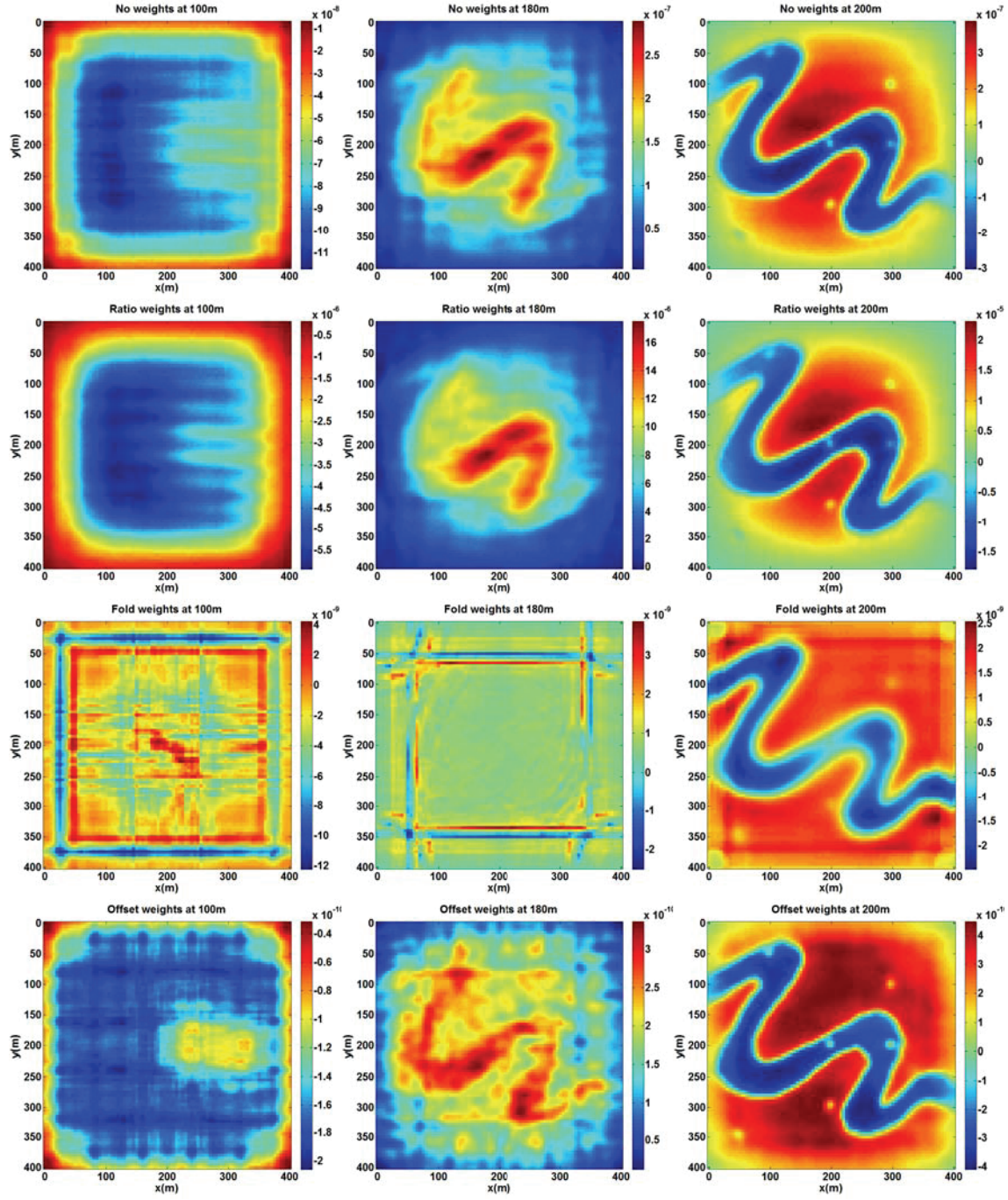


FIG. 13. Prestack-migrated depth slices at 100m (left), 180m (middle), and 200m (right) for the survey with removed shots. Top to bottom: no weights (reference), delta-ratio weights, delta-fold weights, and common-offset weights.

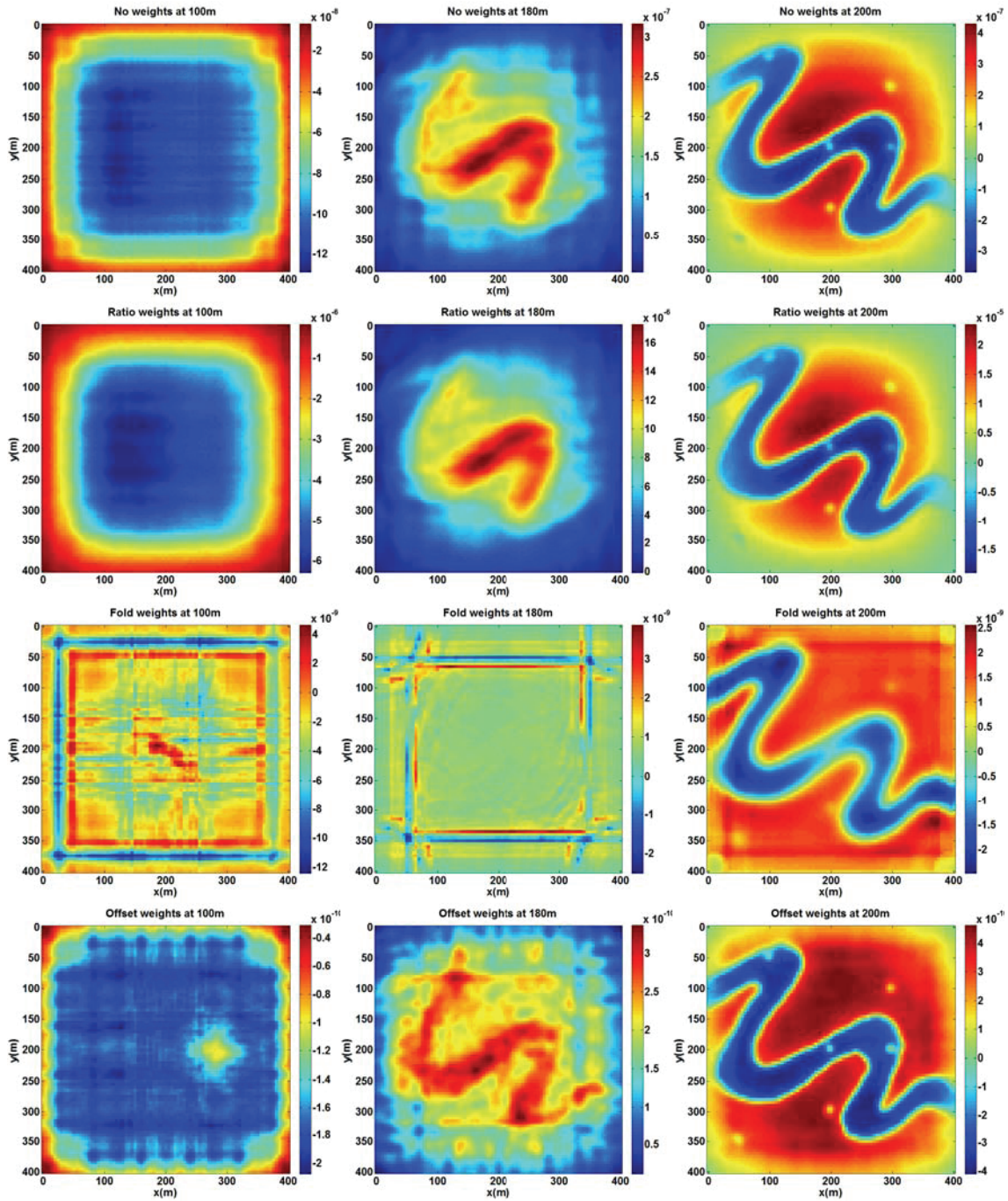


FIG. 14. Prestack-migrated depth slices at 100m (left), 180m (middle), and 200m (right) for the survey with skidded shots. Top to bottom: no weights (reference), delta-ratio weights, delta-fold weights, and common-offset weights.

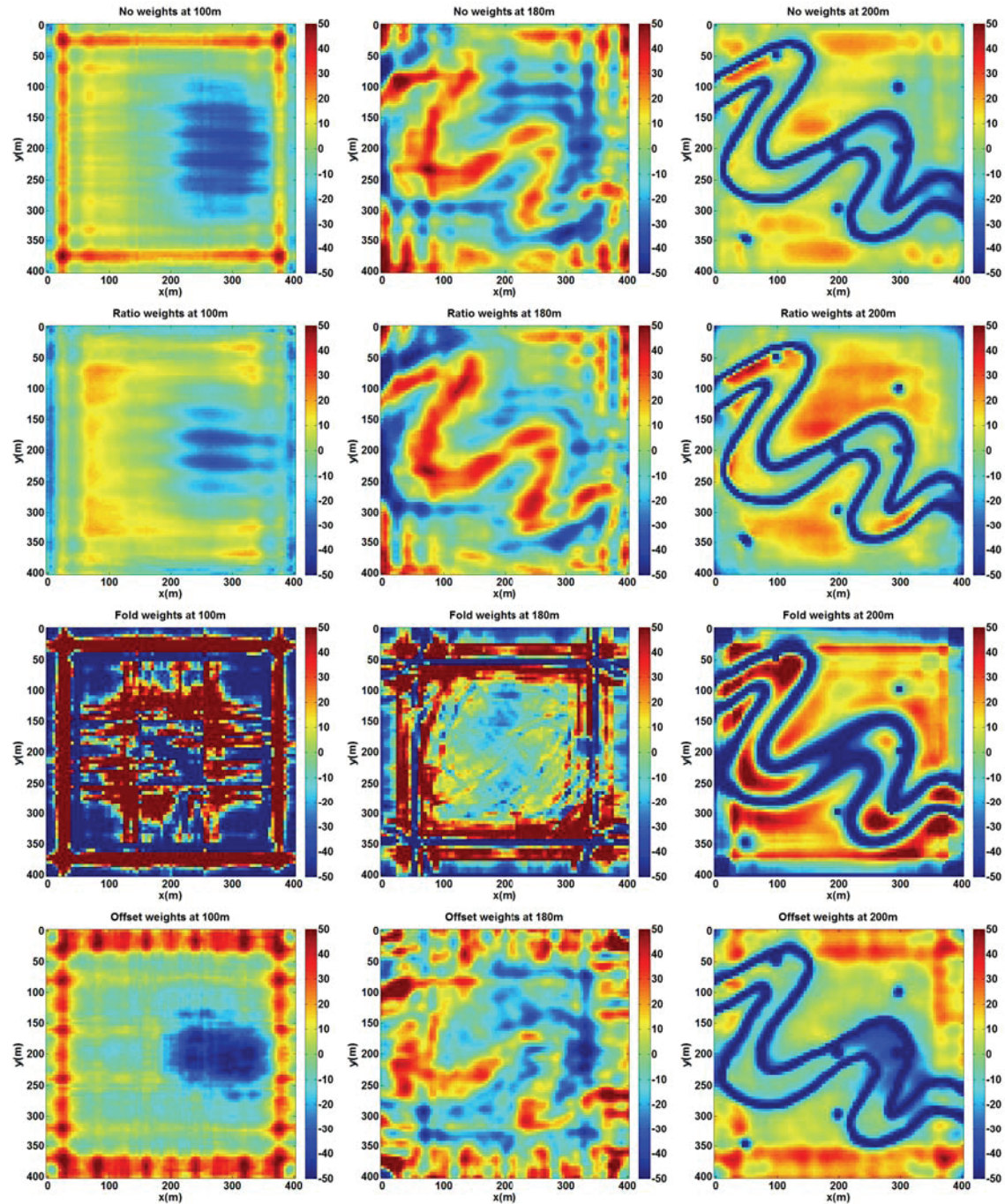


FIG. 15. Percent difference between migrated depth slices and the true reflectivity at 100m (left), 180m (middle), and 200m (right) for the survey with removed shots. Top to bottom: no weights (reference), delta-ratio weights, delta-fold weights, and common-offset weights.

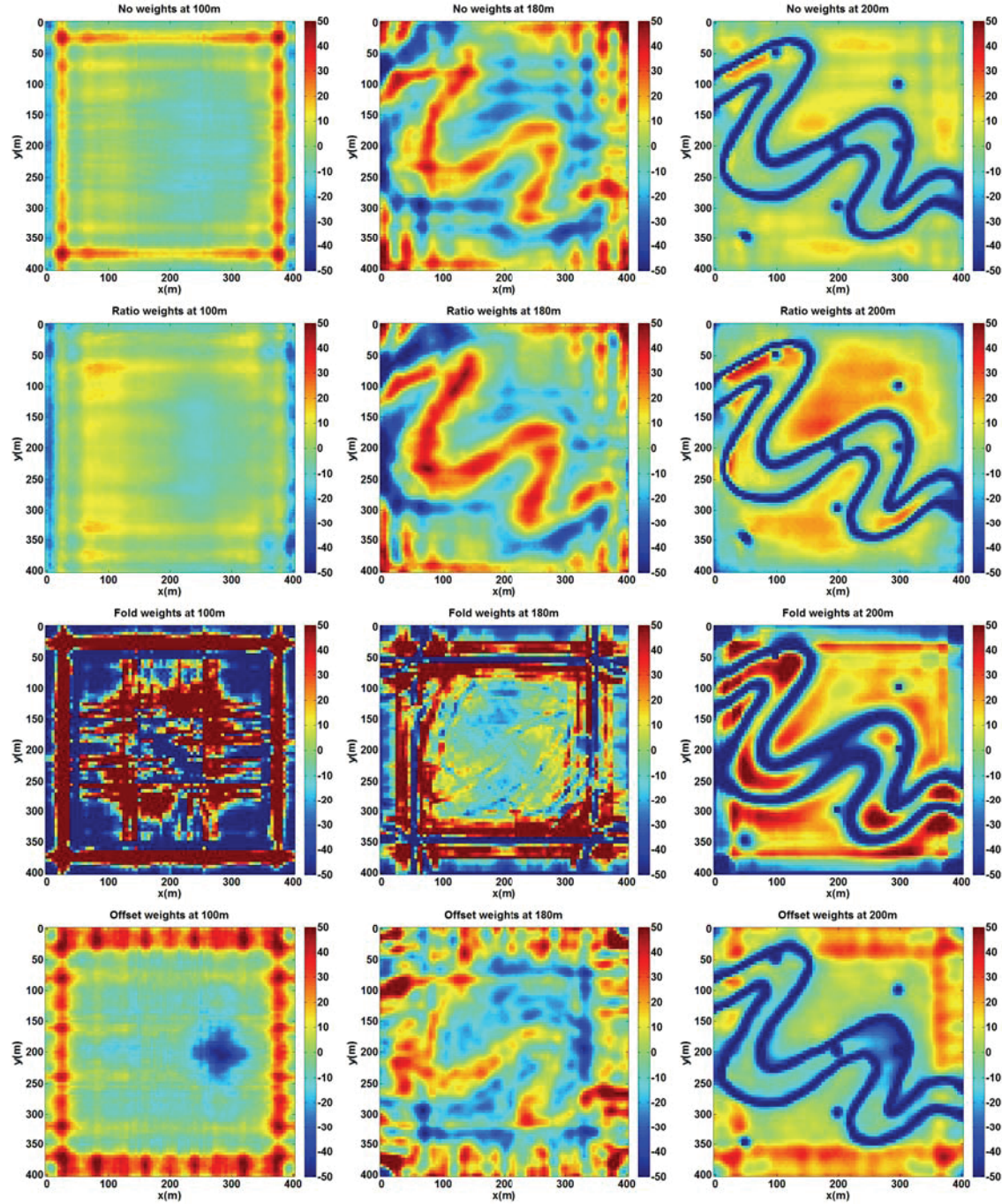


FIG. 16. Percent difference between migrated depth slices and the true reflectivity at 100m (left), 180m (middle), and 200m (right) for the survey with skidded shots. Top to bottom: no weights (reference), delta-ratio weights, delta-fold weights, and common-offset weights.

DISCUSSION AND CONCLUSIONS

In these simulations, delta-ratio weights helped reduce internal footprint artefacts when compared to a migration algorithm that did not include additional weights. The method also performed better than an implementation of a more conventionally used common-offset weighting scheme. Delta-ratio weights do not compensate for the

aperture imprint of the survey, but it may be possible to use another method for aperture compensation, as was attempted in this study. In contrast, delta-fold weights and common-offset weights do remove the aperture effect. However, fold weights appear to reduce spatial resolution in the migrated images and overall do not produce good images. This may be slightly surprising since delta-fold weights make some intuitive sense; if delta-ratio weights which involve dividing hit counts from an *aperture-limited* exhaustive survey by decimated hit counts reduce internal footprint but do not compensate for aperture, then perhaps dividing hit counts from an *infinite-aperture* exhaustive survey by decimated hit counts would compensate for aperture while still producing the footprint reduction. This is not the case, though, since this second case is the same as delta-fold weighting, since an infinite-aperture exhaustive survey would have an equal (infinite) number of hits in every delta bin.

As shown in the simulations by Cooper et al. (2007), common-offset weights can produce much better images than those shown in this study, when implemented in an industrial-strength algorithm. However, the same methods of weight smoothing and borrowing of traces from adjacent bins included in such an algorithm, could also be implemented in a delta weighting algorithm, and would likely result in improvements for that method as well. In addition, both methods could be applied with a different choice of binning, which could also produce improvements. One advantage of the delta-ratio weights over common-offset weights is that the common-offset weights are strictly a midpoint concept, and as such are depth independent and are limited to flat reflectors. The delta-ratio weights are image-point based, and as such they can vary with depth and can apply to any dip.

The images of the decimated datasets produced by all of the migration algorithms display footprint artefacts. This emphasizes the importance of proper sampling of the seismic wavefield during acquisition, and demonstrates that processing, prestack migration in particular, cannot be relied upon to completely compensate for poor sampling. In the case of a hole in the survey, the survey with smooth variations in shot positions produced better images than the survey with abrupt gaps in the shot lines, though the first case did involve more total shots than the second case, and as such may not be an ideal comparison. Despite the inability of prestack migration to suppress all footprint artefacts induced by the decimated survey geometries, the delta ratio weights do have a theoretical and intuitive foundation and they produce some improvement in the images, which suggests that future work is warranted.

ACKNOWLEDGEMENTS

We would like to thank the industrial sponsors of CREWES and POTSI. In addition, the Natural Sciences and Engineering Research Council of Canada (NSERC) and the Alberta Ingenuity Fund (AIF) provided financial support for this project.

REFERENCES

- Bleistein, N., J. K. Cohen, and J. W. Stockwell, Jr., 2001, Mathematics of Multidimensional Seismic Imaging, Migration, and Inversion: Springer.
Cooper, J. K., G. F. Margrave, and D. C. Lawton, 2008, Footprint reduction by angle-weighted stacking after migration: CREWES Research Report, **20**, 38.1-38.23.

- Cooper, J. K., G. F. Margrave, and D. C. Lawton, 2007, Simulations of seismic acquisition footprint: CREWES Research Report, **19**, 28.1-28.20.
- Margrave, G. F., and J. K. Cooper, 2007, Seismic Modelling in 3D for Migration Testing: CREWES Research Report, **19**, 23.1-23.24.